fluids

MDPI

Article

Evaluation Model of Microhemodynamics in Finger Skin at Arterial Occlusion and Post-Occlusive Hyperemia

Andrey P. Tarasov *, Vasily N. Karpov and Dmitry A. Rogatkin *

Moscow Regional Research and Clinical Institute ("MONIKI"), 129110 Moscow, Russia
* Correspondence: tarasov.ap@phystech.edu (A.P.T.); rogatkin@medphyslab.com (D.A.R.)

Abstract

The development of optical noninvasive methods for assessing the functional state of peripheral vessels, including the microcirculatory vascular bed, requires advances in modeling peripheral hemodynamics in order to interpret diagnostic data in terms of vascular tone, wall stiffness, and other related parameters. This study proposes a simple theoretical evaluation model of the dynamics of skin perfusion by blood during a functional test with brachial artery occlusion. As a development of conventional volume-chamber and pressure-volume approaches, this study introduces a problem-oriented three-chamber hemodynamic model of an arm, which allows simulating blood circulation during occlusion of major brachial veins and arteries. The model describes the Poiseuille flow of incompressible viscous blood in vessels with compliant walls, the lumen area of which is regulated by internal blood pressure and vascular tone. The initial diagnostic data for model validation were obtained in clinical trials with the use of the incoherent optical fluctuation flowmetry technique. Comparison of clinical and theoretical results revealed a fundamental qualitative agreement. In this field of medical diagnostics, for the first time, the dynamics of optical signals during the occlusion were successfully interpreted and substantiated as a response to changes in blood pressure and vascular tone in the microcirculatory system.

Keywords: photoplethysmography; blood pressure; occlusion; microhemodynamics; vascular tone; blood volume; theoretical modeling

Academic Editor: Fang-Bao Tian

Received: 2 October 2025
Revised: 20 November 2025
Accepted: 28 November 2025
Published: 30 November 2025

Citation: Tarasov, A.P.; Karpov, V.N.; Rogatkin, D.A. Evaluation Model of Microhemodynamics in Finger Skin at Arterial Occlusion and Post-Occlusive Hyperemia. *Fluids* **2025**, *10*, 314. https://doi.org/10.3390/fluids10120314

1. Introduction

The cardiovascular system is one of the most vital life-supporting systems of the human body. Cardiovascular diseases are recognized as one of the leading causes of mortality; therefore, methods for assessing the condition of the cardiovascular system are of unquestionable relevance [1]. Although nowadays physicians have at their disposal a wide range of instrumental diagnostic tools for evaluating the state and functioning of the heart and vessels (ultrasound, ECG, CT, etc.), not all clinical needs can be fully addressed by these methods. This is especially true for the assessment of microhemodynamics, as well as the functional state of small peripheral vessels, including the microcirculatory system. Due to the small diameter of veins, capillaries, and arterioles, many powerful existing diagnostic tools (e.g., ultrasound) are not applicable in this context [2].

In recent decades, for this reason, research on microhemodynamics using noninvasive optical methods has become a central focus of many scientific groups worldwide. Among these methods are laser Doppler flowmetry (LDF), photoplethysmography (PPG), optical fluctuation flowmetry (OFF), as well as techniques of laser speckle contrast analysis (LASCA) and imaging approaches [3–6]. Importantly, the most reliable and informative

results are obtained when these techniques are combined with functional or provocative tests targeting the microcirculatory system—such as thermal stimulation, occlusion tests, and others [7]. Such test interventions elicit adaptive vascular responses, which allow for a more comprehensive assessment of the regulatory mechanisms in the microcirculatory system, as well as the functional state of vessels themselves, including their stiffness, compliance, and reactivity [8–10].

Occlusion of the brachial artery is also employed as the general test procedure in the oscillometric method of blood pressure (BP) measurement in modern automatic and semi-automatic BP monitors with brachial cuff [11]. Furthermore, the analysis of the sphygmogram waveform (that is, the contour of the envelope of pulse-induced air oscillations in the cuff) during the de-compression of the brachial artery is only the technique used in all BP monitors to indirect determine of BP [12,13]. At the same time, the intrinsic properties of the artery, such as its individual tone, reactivity, wall's elasticity, etc., must a priori influence the final measurement outcome under this technique. However, conventional and commercially available automatic BP monitors do not account for these individual arterial properties. A uniform calculation algorithm is applied to all patients regardless of their individual vascular characteristics, which often results in inaccurate BP readings [12,14].

One of the reasons of such a situation is the absence of analytical models that account for vascular properties during BP measurement, as well as the lack of diagnostic tools for determining individual vascular parameters in vivo that could be incorporated into such models during the measurement process. The integration of BP monitors with optical methods for in vivo assessment of vascular properties (PPG, OFF, etc.) provides a promising approach to addressing this problem. The key unresolved challenge, however, remains the absence of effective problem-oriented theoretical models of peripheral hemodynamics (particularly in skin of extremities), as well as methodologies for interpreting registered optical signals in terms and parameters of these models. Therefore, the development of such models and methodologies is an important scientific task.

In general, since the late 1980s, a number of physical models have been proposed to describe the dynamics of blood flow and pulse wave propagation in vessels during brachial artery compression by a BP monitor's cuff [15–19]. The data processing algorithms to obtain BP values are typically based on mathematical simulation models which describe the air pressure pulsations in the cuff, induced by blood pulsations in the compressed brachial artery. These models analyze the waveform envelope of the sphygmogram signal (air pressure oscillations in the cuff) as a function of BP and blood pulsations in the brachial artery during the inflation or deflation of the cuff. Such models provide a rationale for the generation of the oscillometric signal and make it possible to simulate various scenarios. A number of modern modifications of these models have also been reported [20,21]. However, all of them fail to describe the more general hemodynamics and microhemodynamics in the skin of the arm during BP measurement and under prolonged brachial artery occlusion of up to 3 min, as is typically employed in the standard functional test [7]. At the same time, it is precisely this test enables both qualitative and quantitative assessment of vascular tone and reactivity [10].

A number of studies have also investigated the behavior of PPG signals during BP measurement using the oscillometric method with a brachial cuff, including attempts to improve the accuracy of BP measurement by automatic monitors [22–24]. However, these studies do not present mathematical models linking PPG signal behavior with vascular stiffness, tone, and/or other properties, as well as do not address the modeling of microhemodynamic changes in hand skin at a test with occlusion. To the best of our knowledge, no previous work (including our own) has provided a theoretical explanation of the behavior of the PPG signal recorded from the finger skin during long-term (up to 2–3 min) arterial

occlusion, accounting for the dynamics of vascular tone during brachial compression. Traditional PPG or LDF techniques do not provide such information due to the fact that they do not analyze quasi-static components of optical signals. Their readings usually fall down to zero at arterial occlusion.

A number of studies have specifically analyzed the quasi-static components of PPG or LDF signals [25–27]. In some instances, such as [25], the research objective is to investigate perfusion changes in response to various provocations, including respiratory, cold, or thermal challenges. However, this represents a distinct research direction; it does not focus on perfusion dynamics during and after vascular occlusion.

In some cases, occlusion itself is the subject of the study, and articles contain published dependencies of the experimentally recorded dynamics of the quasi-static component of optical signals throughout long-term occlusion. The typical aim in these cases is to compare the signal immediately before occlusion onset with that during the post-occlusive reactive hyperemia (PORH) phase, i.e., after the end of occlusion. Crucially, they often omit a detailed interpretation of the signal dynamics throughout the occlusion period itself and do not assess the altered blood flow in the occluded limb as the cause of the observed optical signal changes. For example, ref. [26] studies the correlation between ultrasound-measured flow-mediated dilation of the brachial artery and the PPG signal in response to occlusion.

The objective of the present study is to provide a qualitative mathematical description of the PORH phenomenon, coupled with an analysis of blood flow redistribution in the finger skin during prolonged occlusion, taking into account vascular tone and reactivity. As a preliminary step, the aim was not to achieve a high-accuracy quantitative description of blood flow or the corresponding PPG signals, but rather to establish an acceptable qualitative interpretation.

Thus, the paper introduces a simple evaluation model to simulate microhemodynamics in finger skin before, during and after brachial occlusion using a brachial cuff. Also, a distinctive feature of this model is that it accounts for cuff compression of both the arterial and venous systems of the upper limb, as well as for the tone of arterial and venous vessels. These aspects and subsequent development of PORH in the skin microvascular bed are rarely addressed in other models. Under normal conditions, as part of the adaptive vascular response to acute ischemia and hypoxia, vascular tone begins to decrease sharply immediately after occlusion is released. In the initial moment following cuff release, this typically results in a pronounced increase in blood perfusion inside skin (hyperemia), compared with the pre-occlusion baseline. Indeed, the assessment of the perfusion magnitude and the perfusion growth rate during PORH is commonly used in optical flowmetry techniques (LDF, OFF, etc.). However, our approach models blood flow in skin not only at the moment of PORH, but also over the entire time interval of several minutes—before the onset of occlusion, throughout the occlusion period, and during the post-occlusion phase. This opens up new diagnostic perspectives.

The theoretical results are supported by real clinical data, which allow their interpretation in terms of vascular tone dynamics, both under normal conditions and in the context of age-related vascular changes and/or vascular pathologies. It should be specially noted that the direct study of differences in optical signals behavior across various vascular diseases was not the aim of this study, and so no systematic data of this type were presented here. This will be the subject of future investigations. In the present paper, real clinical data are used solely as basic demonstrative (training) examples, which make it possible to qualitatively test the model and outline future research directions.

2. Materials and Methods

2.1. Clinical Data

In the clinical part of the study, raw data arrays for BP and PPG signals were obtained using a prototype device called "Vasotest" [28,29]. The core of the Vasotest device is a module of an automated BP monitor that measures BP using the well-known oscillometric method with a brachial cuff. The device also includes a compact electronic unit with an internal microcontroller and external optical sensors, which can be attached to the patient's extremities. The external optical sensors simultaneously implement PPG and OFF technologies [5] and are designed to provide information about peripheral microhemodynamics. Diagnostic data are recorded, stored and processed with the use of a physician's personal computer (Figure 1a). In the described study, one optical sensor operating in the reflection mode was used. It was attached to the distal phalanx of the index finger (Figure 1b).

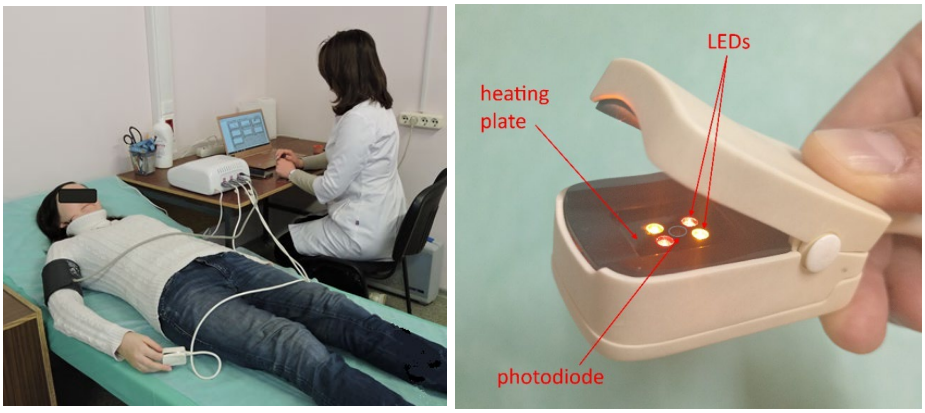

(**a**) (**b**)

Figure 1. Prototype of diagnostic device: (**a**) examination procedure and (**b**) optical PPG sensor for finger.

For optical measurements, each sensor employed LED light sources emitting in the 560–590 nm wavelength range, covering the isosbestic points of hemoglobin [28]. The signals were detected by a silicon photodiode positioned in the center of the sensor (Figure 1b), ensuring maximum sensitivity to skin blood volume oscillations [30]. The integrated automated BP monitor, in addition to standard systolic (SBP) and diastolic (DBP) BP measurements, can, under computer control, automatically induce brachial artery occlusion for up to several minutes.

To ensure thermal stabilization of the measurement site (skin), each optical sensor was equipped with a heating plate and a temperature sensor located beneath the sensor surface (Figure 1b), maintaining skin temperature in the range of 32–33 °C during all baseline measurements. All device operations, diagnostic data acquisition, and processing were carried out according to a specially developed diagnostic algorithm implemented in the device software, created in the LabView environment (National Instruments Corp., Austin, TX, USA).

During examination, the patient was positioned lying on a couch. The PPG sensor was attached to the index finger, and optical signals were recorded from the distal phalanx on the palmar side. The BP monitor cuff was placed on the upper limb in the standard manner. The measurement procedure consisted of several phases. In this study, Phase 1 involved recording the baseline PPG signal without intervention for the initial 40 s. This was followed by Phase 2, brachial artery occlusion, lasting 2 min with cuff air pressure standardized for all subjects at 200–220 mmHg, and finally Phase 3, observation of post-occlusion reactive hyperemia (PORH) for 2–3 min. A typical "raw" optical signal recorded

from a conditionally healthy subject is shown in Figure 2. The vertical axis in Figure 2 represents the amplitude of the photodiode signal after amplification (in volts), and the horizontal axis shows the test duration in seconds. Cuff inflation began at 40 s, and cuff pressure was released at maximum speed at 160 s.

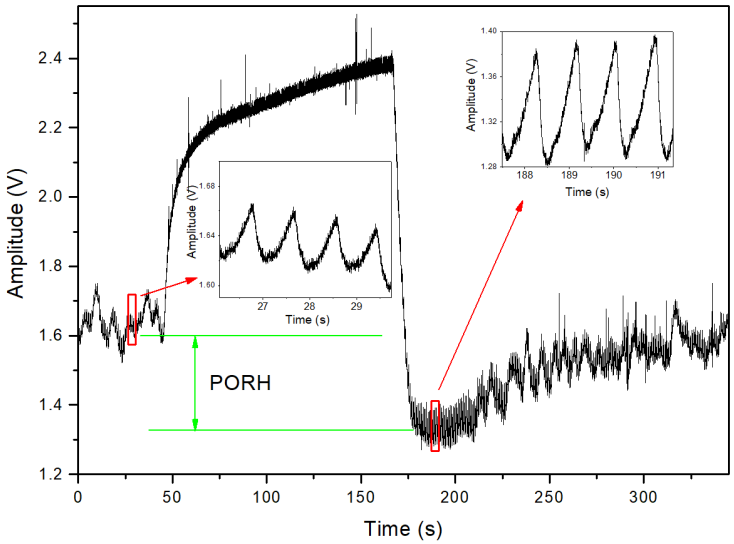

Figure 2. Raw signal recorded by the PPG sensor before, during, and after occlusion. Occlusion starts at 40 s and ends at 160 s. The optical signal reduction at the moment of PORH is clearly visible.

It should be emphasized that the signal presented here is not a standard PPG waveform, but rather the raw signal directly recorded by the photodiode—without filtering or removal of the slowly varying DC component (signal bias). For the purposes of this study, we focus specifically on analyzing and modeling the behavior of this raw signal. A standard PPG waveform can be derived from the raw signal by band-pass filtering in the 0–5 Hz range. Such signals have been analyzed during occlusion in previous studies, e.g., [22]. They are well registered before occlusion, show an increase in amplitude during PORH, but disappear completely during occlusion, as blood supply and pulsations in the skin are blocked; therefore, they contain no information about hemodynamics during the occlusion phase. By contrast, the raw signal, as will be shown below, carries rich information about vascular function and the redistribution of blood within the vascular bed during occlusion.

Since probing optical radiation in the isosbestic wavelength band of 560–590 nm is strongly absorbed by blood hemoglobin, the greater the blood filling within the diagnostic volume of finger skin, the lower the signal amplitude registered by a photodetector. The dependence is not linear; however, as we recently demonstrated in [31], the recorded signal can be readily converted into the relative blood volume V_b in the skin if the optical properties of the tissue are known. In particular, in [31] it was shown that within a relatively narrow interval of V_b (~0.05 rel. units), the following expression holds for the relative backscattered flux F:

$$F(V_b) = F_0 e^{-\varepsilon V_b}, \quad (1)$$

where F_0 and ε are coefficients. In particular, for V_b in the range 0.05–0.1, $F_0 = 8.21 \times 10^{-7}$ and $\varepsilon = 51.6$; for V_b in the range 0.1–0.15, $F_0 = 4.31 \times 10^{-7}$ and $\varepsilon = 44.9$, assuming the skin optical parameters taken in [31].

Based on Equation (1), it is possible to estimate the range of changes in the relative volumetric blood filling level V_b for the entire raw PPG signal. To do this, the mean level of V_b at the initial time point is determined from the average signal level (excluding blood pulsations). Typical values for the fingertip lie in the range of 0.1–0.2. Then, using Equation (1), the recalculation $\Delta F(V_b) \rightarrow \Delta V_b$ is performed. As an example, Figure 3

shows the time dependence of the PPG signal (taken from Figure 2) compared with the corresponding V_b values. It can be seen that while the PPG signal amplitude increases by ~50%, the change in V_b amounts to only ~8%.

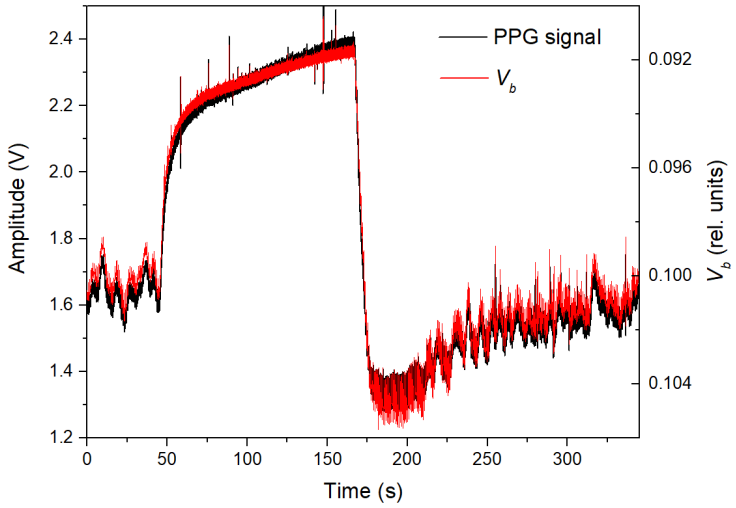

Figure 3. Raw PPG signal and recalculation of signal amplitude into relative blood volume V_b.

In this study, since the focus is on a qualitative model, precise quantitative values of V_b were beyond the scope of our objectives. Therefore, they are not further presented or analyzed in Section 3 for the test clinical data. Nevertheless, we considered it important to note here the feasibility of such recalculation for future investigations in this direction. In fact, an analogous approach is well known in tissue oximetry, where in addition to blood oxyhemoglobin saturation, total hemoglobin is also evaluated, including during the performance of an occlusion test [32].

2.2. Theoretical Approach

Hemodynamics in blood vessels is an extremely complex and multifactorial process. A precise model of hemodynamics—especially in small peripheral vessels, accounting for all anatomical details of the vasculature (tortuosity, arteriovenous shunts, etc.), regulation of vascular tone, and the cellular composition of blood as a complex biological suspension (e.g., erythrocyte aggregation)—is unlikely to emerge in the near future. All modern models rely on certain simplifications and are, for the most part, qualitative rather than quantitative. The most commonly reported simplifications include treating blood as an incompressible Newtonian fluid, assuming laminar flow, neglecting vessel tortuosity (bends in the flow, peculiarities of circulation in the elbow or knee joints), and representing vessels and blood flow within them as one-dimensional (1D) structures and processes, among others.

In this study, our aim, as the initial pilot stage, was to formulate and validate a purely qualitative model that provides a simplified description of the behavior of the raw optical signal (as in Figure 2), without attempting any precise quantitative evaluations. Accordingly, within such a model, coarse assumptions are acceptable as long as they allow the research objective to be achieved. The main requirements are maximum simplicity and usability for physicians and medical physicists, while ensuring the possibility of interpreting diagnostic data in terms of vascular tone and reactivity of the peripheral vascular bed.

Based on these considerations, we used for our vascular model of the upper limb the well-known volume-chamber and pressure-volume approaches [33], adapted to the problem of describing hemodynamics in an arm during brachial artery occlusion. We proposed a simple, problem-oriented three-chamber hemodynamic model of the arm's

vascular bed, with the ability to simulate compression of major veins and arteries. The model describes Poiseuille flow of incompressible viscous blood (Newtonian fluid) in vessels with compliant walls, whose lumen area is regulated by both BP and vascular tone. The chamber model of blood vessels originates from the Chamber model by Frank [34], which treats blood vessels as elastic reservoirs whose volume is a function of BP inside them, owing to the high compliance and elasticity of their walls. Following the ideas by Frank and other well-known model representations of the problem, we consider the brachial artery as the first chamber; the skin microvasculature as the second chamber; and the venous bed as the third chamber (Figure 4).

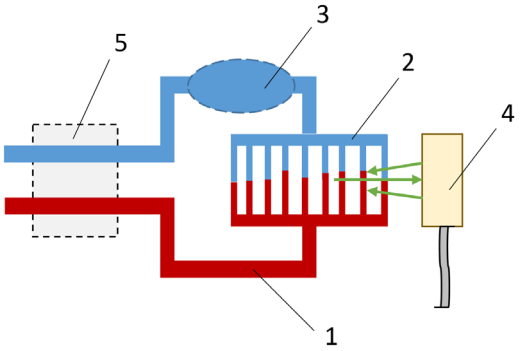

Figure 4. Three-chamber model of the arm vascular network. 1—arterial chamber. 2—chamber of small vessels and microvascular bed. 3—venous chamber. 4—remote optical probe. 5—brachial cuff.

It should be emphasized that the optical signal is recorded from the microvascular chamber, where blood perfusion may exhibit dynamics that, in general, differ from hemodynamics in large vessels. Capillaries play a major role here, and the physics of blood flow in capillaries is distinct from that in larger vessels. Here, not only blood flow obeys fundamentally different physical laws compared to large vessels, but here is also specific transcapillary exchange of blood components with surrounding tissues (part of the plasma leaves the vessels, deoxygenation occurs, viscosity changes). Description of all these processes within a single model is extremely complex. Therefore, we do not explicitly model the capillary blood flow, but rather consider the overall hemodynamics through the chamber as a whole.

In the general case, blood flow in an individual vessel with compliant walls can be described by the well-known system of equations that includes the Navier–Stokes equation, which describes the motion of a viscous Newtonian fluid under the action of pressure forces and forces of viscous friction, the equation of continuity of a flowing fluid in the vessel with compliant walls, and the equation of state of the vessel (see, for example [35]). The last equation describes a dependence of the vessel's lumen area S on the pressure applied to the vessel's walls P and can be formulated, in general, as:

$$S = S(P). \tag{2}$$

As is known, such a system of equations can, in principle, describe linear blood flow (both laminar and turbulent) with the linear velocity of blood flow v, as well as the propagation of two types of waves: fast acoustic waves, which generate the Korotkoff sounds, and slow pulse waves. In this work, we are specifically interested in slow pulse waves registered by PPG. To describe them, the wave equation is usually derived from the specified system of equations (see, for example, [18]), the main parameter of which is the

pulse wave velocity v_{PW}, which, in turn, can be determined by the known Bramwell and Hill equation:

$$v_{PW} = \sqrt{\frac{S}{\rho} \cdot \frac{\partial P}{\partial S}}. \tag{3}$$

where ρ is the blood density.

Equation (3) is of particular importance as it introduces a key quantity: the partial derivative $C = \partial S/\partial P$, which characterizes the compliance of the vessel's wall. For modeling purposes, it is highly desirable that the equation of state permits an analytical, explicit form for the compliance, C. Such a formulation significantly simplifies the selection of vascular elasticity parameters within the region of maximum compliance and the estimation of pulse wave velocity.

A major challenge in hemodynamics is the lack of exact solutions to its governing equations and the considerable difficulty even in obtaining approximate solutions. Therefore, in practice, numerous simplifying assumptions or more straightforward estimation methods are often employed.

One of such estimation methods is the use of the well-known exact stationary solution of the Navier–Stokes equations known as the Poiseuille equation. It describes the stationary blood flow Q through a single vessel with a known pressure difference ΔP between the inlet and outlet of the vessel [34]:

$$Q = \frac{\Delta P}{R}, \tag{4}$$

where R is resistance to blood flow and $\Delta P = P_{in} - P_{out}$. Resistance R is determined through blood viscosity μ, vessel radius r and length l as $R = 8\mu l / \pi r^4$, therefore R can be roughly expressed through the lumen area of the vessel S as follows:

$$R = \frac{8\pi\mu l}{S^2}. \tag{5}$$

This approach makes it possible to estimate the blood flow through the section of the brachial artery and veins of the arm under the cuff at different air pressures inside the cuff and at different vessel lumen areas S. For example, with $S = 40$ mm^2, $l = 100$ mm (the width of the BP monitor cuff) and $\mu = 4 \ldots 5$ mPa·s, calculated R is $0.0063 \ldots 0.0079$ Pa·s/mm^3. During cuff inflation, R is increasing rapidly, completely blocking blood flow when $S \longrightarrow 0$.

Using such a quasi-stationary approximation and assuming that the linear velocity of blood flow v does not change significantly over the time interval Δt, the change in blood volume V_b in any chamber can be determined over Δt as follows:

$$V_b(t + \Delta t) = V_b(t) + (Q_{in} - Q_{out})\Delta t, \tag{6}$$

where Q_{in} and Q_{out} is the inlet and outlet blood flow for the chamber. By introducing the average effective length of the chamber's vessels $\widetilde{l}$ as a constant in the model, one can find a new average vessel's lumen area S in the chamber:

$$S(t + \Delta t) = \frac{V_b(t + \Delta t)}{\widetilde{l}}. \tag{7}$$

Subsequently, the new average pressure in the chamber, $P(t + \Delta t)$, can be computed, provided the explicit form of the equation of state (Equation (2)) and its corresponding inverse function are known.

In line with common practice in models simulating pulse waves within the cuffs of automatic BP monitors, we employed a suitable equation of state. In particular, we utilized

the exponential model proposed in [36,37], which has been widely adopted in oscillometric research [17–19]:

$$S(t) = \begin{cases} S_0 e^{aP(t)}, & P(t) \le 0 \\ S_{max} + (S_0 - S_{max}) e^{-bP(t)}, & P(t) \ge 0 \end{cases}, \quad (8)$$

where S_{max} is the maximum possible vessel lumen area at physiological values of pressure $P(t)$ acting on vessel walls, S_0 is the vessel lumen area at $P(t) = 0$, and the coefficients a and b characterize the elastic properties of the vessel wall. At the same time, for integration to be possible, the following condition must be satisfied:

$$a = b\left(\frac{S_{max}}{S_0} - 1\right). \quad (9)$$

Since, from a diagnostic perspective, as noted above, we are not interested in blood flow velocity and movement, but rather in the relative blood volume fraction $V_b(t)$ within the diagnostic volume of the skin (in the microcirculatory chamber), the state Equation (8) together with Equations (4)–(7) are quite sufficient for an approximate numerical (stepwise) solution of this problem.

As previously outlined, we considered the three-chamber hemodynamic model of the arm's vascular bed (Figure 4). To implement the system defined by Equations (4)–(9), initial conditions for pressure $P_i(0)$, blood volume $V_{bi}(0)$, and lumen area $S_i(0)$ must be specified for each chamber i (i = 1, 2, 3).

The model incorporates resistive elements R_i at the output of each chamber, which govern the flow reduction according to Equation (4), given the pressure difference ΔP between the chambers. An additional input resistive element, R_0, is defined at the inlet of the first chamber. The resistances R_1 and R_2 were treated as constants. In contrast, the magnitudes of R_0 and R_3, located at the entrance and exit of the arm's vascular network beneath the compression cuff, were dynamically computed using Equation (5). This formulation accounts for their dependence on the variable lumen area $S(t)$, which is itself influenced by the transient cuff pressure.

Thus, for example, for the first arterial chamber with $P_1(t)$ after the time interval Δt, the change in the blood volume ΔV_{b1} will be determined as:

$$\Delta V_{b1} = \left(\frac{P_a(t) - P_1(t)}{R_0(t)} - \frac{P_1(t) - P_2(t)}{R_1}\right)\Delta t, \quad (10)$$

where $P_a(t)$ is BP at the entrance of the chamber and $P_2(t)$ is BP in the next chamber. This change in volume, with the total vessel length of the chamber remaining constant, leads only to a change in the chamber-averaged total cross-sectional area of vessels ΔS_1, and, hence, to a new instantaneous averaged value $S_1(t)$ in the chamber. Using Equation (8) and setting the constants S_{max} and S_0 for the chamber, the new instantaneous pressure value $P_1(t)$ in the chamber can be easily determined from Equation (8):

$$P_1(t) = -\frac{1}{b}\ln\frac{S_{max} - S_1(t)}{S_{max} - S_0}. \quad (11)$$

By repeating the stepwise process for each chamber, it is possible to construct the entire qualitative picture of the dynamics of pressures and blood volume filling in each chamber during the long-term occlusion test.

To specify the initial blood flow and the pulse wave in the brachial artery, we used the standard synthesis of pulse wave using a Fourier series representation for the arterial pressure with two frequency components [17]:

$$P_a(t) = DBP + \frac{(SBP - DBP)}{3.6}\left(1.8 + \sin\left(2\pi\frac{HR}{60}t\right) + \sin\left(4\pi\frac{HR}{60}t\right)\right), \quad (12)$$

where DBP and SBP are diastolic and systolic BP; HR is the heart rate [min^{-1}]. In this study, we are not interested in phases of the signals, so they are taken to be equal to zero.

A key feature of the proposed model is the attempt to account for vascular tone. For this purpose, the pressure $P(t)$ on the vessel walls for each chamber can be represented as the sum:

$$P(t) = P_b(t) - P_T(t), \quad (13)$$

where $P_b(t)$ is BP, which can be considered as arterial BP $P_{ba}(t)$, venous BP $P_{bv}(t)$, or BP in a microcirculation chamber $P_{bm}(t)$; and $P_T(t)$ is the pressure generated by smooth muscles on the vessel wall. $P_T(t)$ can also be separately specified in the arterial chamber $P_{Ta}(t)$, venous chamber $P_{Tv}(t)$, or microcirculatory bed $P_{Tm}(t)$.

If a section of the vascular bed under a BP monitor cuff is considered, then the cuff air pressure $P_c(t)$ is added to Equation (13):

$$P(t) = P_b(t) - P_T(t) - P_c(t). \quad (14)$$

This pressure $P(t)$ is often referred to as transmural pressure and denoted $P_t(t)$.

The system of Equation (8) also allows explicit analysis of the compliance of the vessels in each chamber if their parameters b, S_{max}, and S_0 are known. Since, in the absence of a cuff ($P_c(t) = 0$), generally $P(t) > 0$, from the second equation of system of Equation (8), we can obtain:

$$C = \frac{\partial S(t)}{\partial P(t)} = -b(S_0 - S_{max})e^{-bP(t)} = b(S_{max} - S_0)e^{-bP(t)} \quad (15)$$

The difference $S_{max} - S_0$ is considered as constant in our model. Therefore, is possible, up to this constant, to construct a graph of the dependence of C on b for different pressures $P(t) > 0$. This graph is shown in Figure 5.

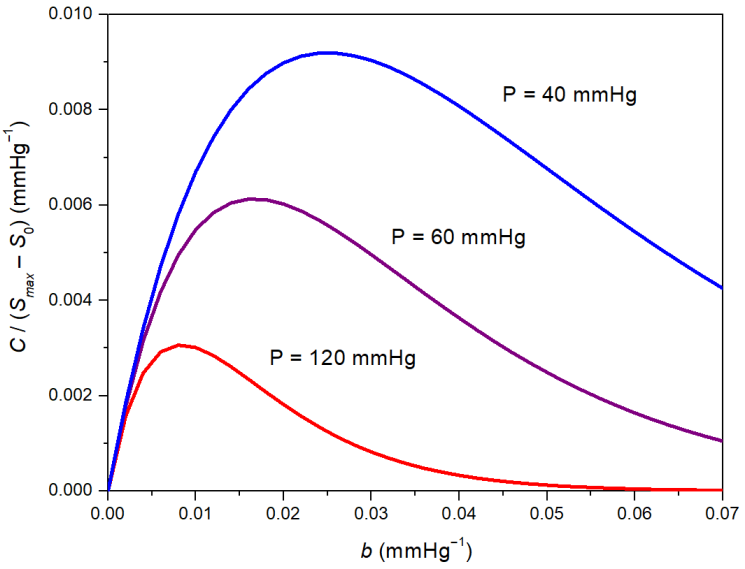

Figure 5. Compliance according to (15) as a function of b for different pressure P.

The global maximum of compliance as a function of b ($dC/db = 0$) is observed under the condition $bP(t) = 1$. We do not claim this with absolute certainty, but as further numerical calculations have shown, the values of b for which the model works well should lie within the range of the compliance maximum. This may indicate that when the elasticity of vessel wall (b) changes, for example, with increasing wall stiffness with age (i.e., decreasing b), the vessel may need to adjust its tone and alter the pressure on the wall to remain near the compliance maximum in order to maintain optimal blood supply. The reduction in muscle tone, particularly in smooth muscles, along with the increase in arterial pressure with age, is generally well documented in human populations [38].

Thus, for the proposed model, for each i-chamber ($i = a, m, v$), the parameters S_{max} and S_0 are specified, values of b near the compliance maximum are chosen, initial values of $P_b(t)$ and $P_T(t)$ are set, and for the transitions $a \to m$ and $m \to v$, the resistances R_m and R_v are assigned, respectively. Additionally, for the input (arterial, a) and output (venous, v) chambers, we set the inlet pressure $P_{a0}(t = 0)$ according to Equation (12), the outlet pressure $P_{v0}(t) = const$, as well as the time parameters and law of change in the cuff pressure $P_c(t)$. After that, a stepwise numerical calculation can be performed over the time interval Δt to determine the changes in pressures and vessel lumen (relative blood volume filling) for each chamber.

It is important to emphasize that the fundamental principles of multi-chamber models and the methodology for step-wise flow calculation have been established since the era of Franck and Poiseuille. Moreover, Poiseuille studied blood flow among other his studies. The novelty of the present model, therefore, lies not in the core methodology, but in its specific adaptations: the application of these established techniques to the particular problem of vascular occlusion and post-occlusive reactive hyperemia; the physiological justification for the parameter b in the compliance expression; and the explicit incorporation of the additional pressure exerted on the vessel walls by vascular smooth muscle (vascular tone).

3. Results

For the purpose of model verification, several dozen signals of the type shown in Figure 2 were recorded from conventionally healthy young volunteers (aged 20–40 years) and volunteers aged 50–80 years. Total number of volunteers was 52. Some of them, including one of the authors of this study, were examined multiple times on different days to ensure reproducibility of the results. For each volunteer, both the left and right sides of the body were examined.

Then, typical signal shapes were selected and grouped, clearly reflecting different hemodynamics in the finger skin during occlusion, in order to test the ability of the model to qualitatively describe and explain the behavior of these signals. Typical signals collected are shown in Figure 6. The most frequently occurring signals were those shown in Figure 6a–c, which reflects more than 50% of cases. Since we are not evaluating an individual volunteer but rather the typical behavior of optical signals, subject-specific data and their physiological analysis was not within the scope of our study. Our interest lied not in a medical diagnostic conclusion, but in the fundamental ability of the model to simulate the recorded typical signal behavior.

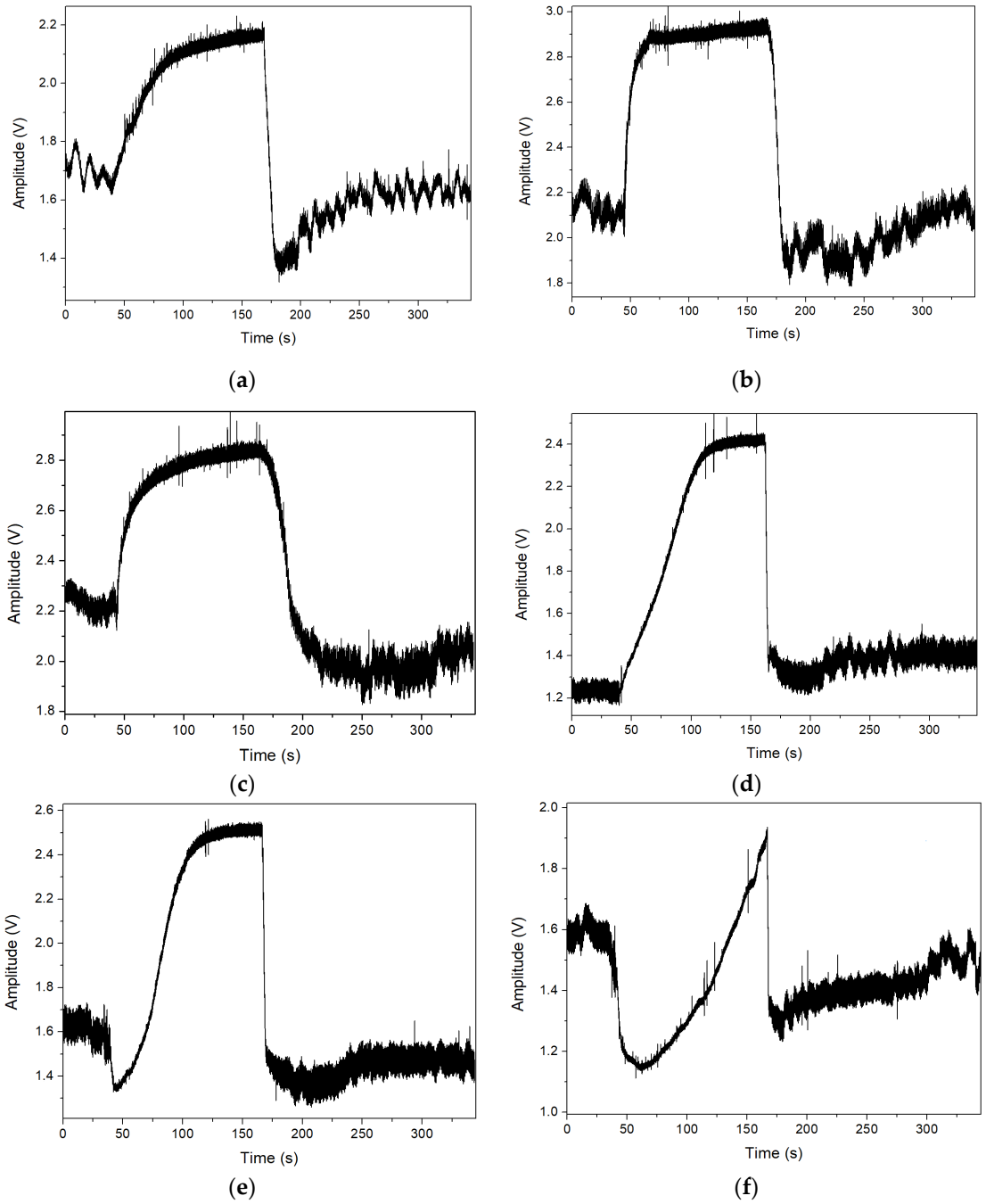

Figure 6. (**a**–**f**) Typical raw PPG signals recorded during an arterial brachial occlusion test.

There are several points to note from the recorded signals before proceeding with the data analysis. A clear general trend of increasing signal amplitude during occlusion is observed in almost all cases, which can only be associated with a reduction in the overall blood perfusion in the diagnostic volume (the larger the volume fraction of blood, the smaller the optical signal, and vice versa). Also, in Figure 6, in almost all cases, after the end of occlusion, the signal is lower than that before the occlusion, indicating the development of PORH. An exception is Figure 6d, where the baseline signal before occlusion is higher. Such cases, as it turned out, also occur in approximately 5% of volunteers (3 persons). The most unusual and unexpected case is shown in Figure 6f. It is characterized by an initially sharp increase in blood perfusion in the diagnostic volume, followed by a decrease and then another increase. A few such cases were also observed for the elderly volunteers, approximately 10% (3 of 26 elderly volunteers). Moreover, such a signal behavior was

observed for one of the authors of this work and it was reproducible several times on different days, which cannot happen if the signal behavior was random. To the best of our knowledge, there are no similar results published in the literature, as well as there is currently no widely accepted explanation for such signal behavior from the vascular physiology point of view. Physicians can only offer very general statements regarding elevated BP, impaired venous outflow, etc., without specific explanations for each case. The theoretical modeling, however, allowed us to study the necessary changes in specific parameters of the vascular network responsible for such signal behavior.

In addition, before presenting the modeling results, it is important to formulate a number of general conclusions obtained during the model treatment. These will help to better understand both the results themselves and the absence, perhaps, of some expected additional results, as well as to avoid potential additional questions that currently have no answer yet.

One of such conclusions is that the model includes many initial parameters that, as it turned out, must be well coordinated from the outset. Otherwise, there will be no stable "blood flow" through the chambers, and after some steps, a number of calculated parameters may exceed physiologically plausible ranges. For example, the vessel lumen area could exceed its maximum allowable value, or BP in any chamber could rise the level above 300 mmHg. However, there is currently no established methodology (as far as we know) for correctly coordinating these parameters. Therefore, we proceeded "by trial and error". The large number of parameters also opens up a wide range of possible affects of individual parameters on the computed results, which could and should be studied in the future. In our study, however, it was not performed due to time constraints and the scope of the study. This remains a task for future research.

A second important conclusion is that our model is, without doubt, just a rough qualitative model, which cannot capture all the nuances of the measured real signals, but only allows simulation of the main trends. Therefore, the resulting calculation graphs are highly idealized and do not fully correspond to clinical recordings. For example, respiratory rhythms in the PPG signal and Mayer waves for BP were not modeled. Moreover, small variations in certain parameters, such as the initial BP values, practically do not affect the simulation results. That is, for different baseline BP—whether elevated or lowered—our model produces essentially the same outcome in terms of interpreting the results of the occlusion test. So, we do not provide different such outcomes here. Nevertheless, in our opinion, the main results obtained satisfy the objectives of the study and show that the key model parameter of the vascular response to occlusion is the vascular tone parameter $P_T(t)$, as well as the character of its temporal change (reactivity).

Figure 7 illustrates the simulated BP at the inlet of the arterial chamber according to Equation (12). The data were obtained for DBP = 82 mmHg, SBP = 117 mmHg, HR = 70 min^{-1}. The pulse pressure (PBP) and HR, as it turned out, practically do not affect perfusion dynamics during and after occlusion, but only influence the values of Q_i. Therefore, these uniform parameters were adopted as constants for further calculations.

Figure 8 illustrates the dynamics of the simulated air pressure in a cuff, indicating the beginning and end of occlusion. The value of $P_c(t)$ after complete vessel lumen occlusion does not further affect the blood dynamics in the vascular bed of the arm. Therefore, in all calculations, it was taken identically as shown in Figure 8.

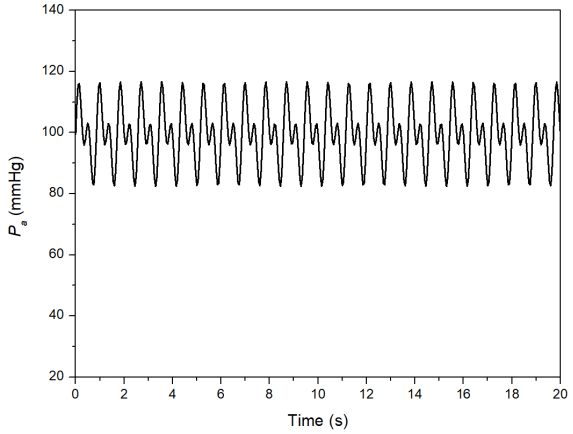

Figure 7. Simulated brachial artery incoming BP.

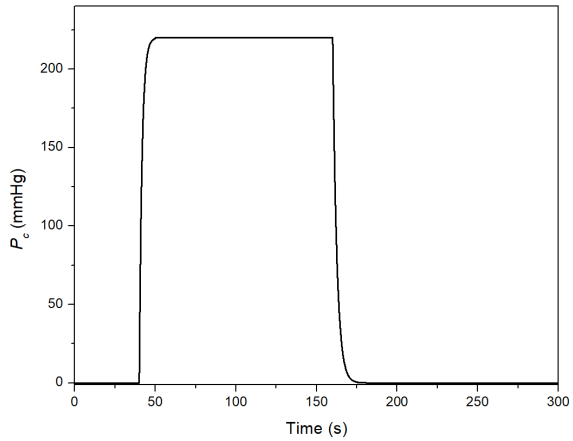

Figure 8. Simulated cuff pressure $P_c(t)$.

With the specified values S_{0a} = 20 mm^2, $S_{max,a}$ = 50 mm^2, b_a = 0.015 mmHg$^{-1,}$ and initial $P_{Ta}(t = 0)$ = 20 mmHg, Figure 9a,b shows the calculated changes in the lumen of the brachial artery before, during, and after occlusion. In the first case (Figure 9a), $P_{Ta}(t) = const$, while in the second case (Figure 9b) it drops sharply to zero at the end of occlusion and then gradually returns to its initial level (similar to the distribution function). The appearance of post-occlusion hyperemia is clearly visible already for the brachial artery in the second case.

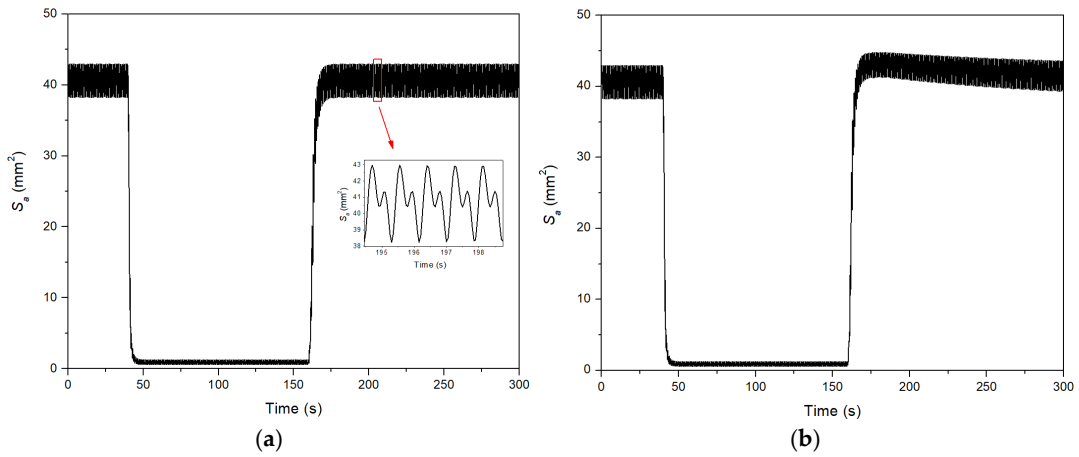

Figure 9. Simulated change in the lumen area of the brachial artery during occlusion: (**a**) arterial tone does not change, smooth muscles pressure P_{Ta} = 20 mmHg; (**b**) arterial $P_{Ta}(t)$ drops sharply to zero at the moment of the end of occlusion (t = 160 s) and then gradually returns to its original state.

Figure 10 demonstrates the main results of blood volume fraction modeling in the skin during occlusion for different typical cases. Unlike Figures 2 and 6, the results here are presented not as an optical signal, but directly in the form in which they are modeled, since the optical signal in volts is not calculated within the model. Such a calculation is possible, for example, using Monte Carlo statistical modeling, as we performed in [31], but this requires knowledge of the individual optical properties of the skin. For the purposes of this study, we considered that there was no need to complicate the results in this way. The main input data for the calculations were as follows: for microcirculation chamber, S_{0m} = 50 mm^2, $S_{max,m}$ = 250 mm^2, b_m = 0.017 mmHg^{-1}, R_m = 8 Pa·s/mm^3, $P_{Tm}(t = 0)$ = 20 mmHg; for venous chamber, S_{0v} = 40 mm^2, $S_{max,v}$= 950 mm^2, b_v = 0.008 mmHg^{-1}, R_v = 5 Pa·s/mm^3, P_{Tv}(t = 0) = 20 mmHg (Figure 10a–c) and 30 mmHg (Figure 10d).

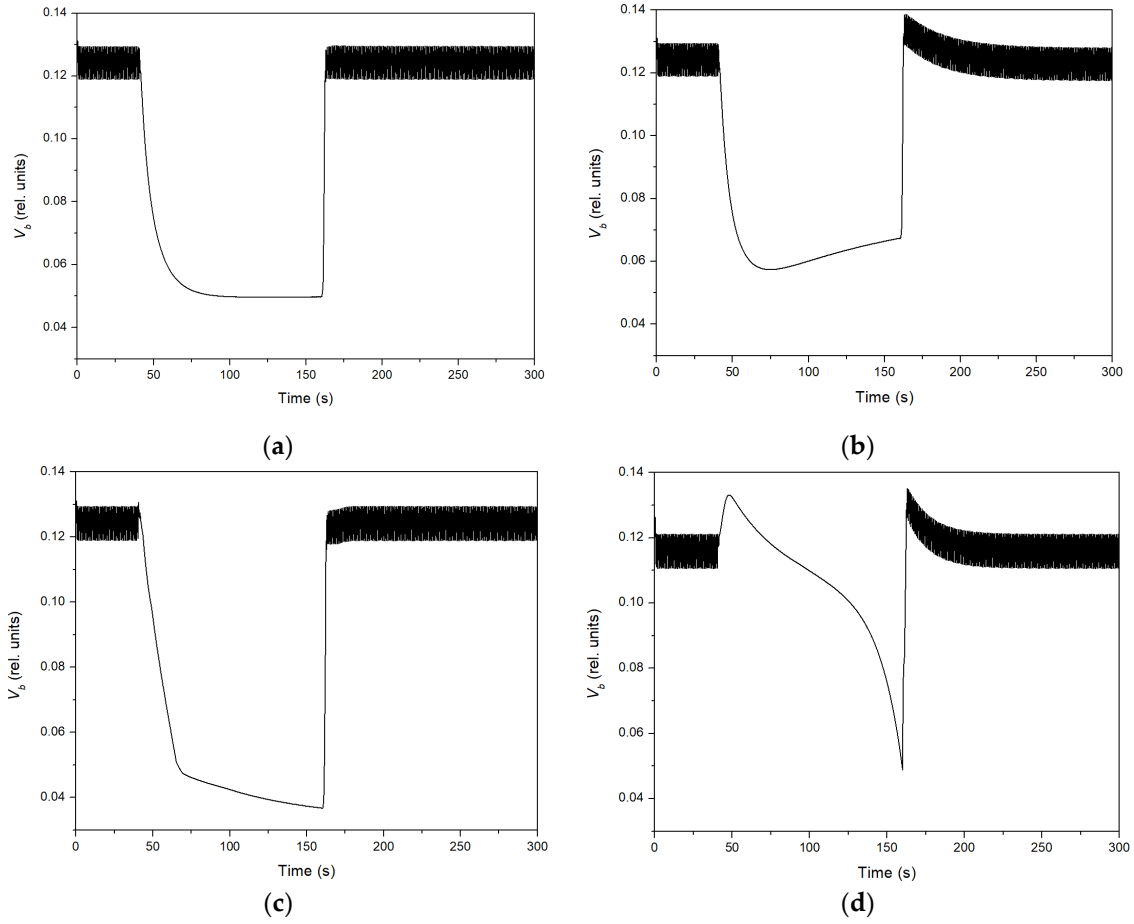

Figure 10. (**a**–**d**) Simulated time dependence of the blood volume fraction V_b in skin.

During occlusion, in theory, only the parameters R_m, R_v and $P_{Ti}(t)$ can change. The main brachial arteries and veins are compressed, so the resistance to blood flow there is maximal, completely blocking circulation. Blood neither flows into nor out of the arm. The elasticity of the vessel walls also cannot change over the course of the experiment. Numerical calculations showed that the reduction in blood filling of the diagnostic skin volume occurs quite rapidly due to the transfer of arterial blood and blood from the microcirculatory bed into the venous chamber, which has the greatest elasticity and the lowest BP. It is well known that veins can increase their volume several times due to blood filling [34,38]. In this model, only vascular tone can effectively influence this process, shaping the dynamics of blood filling as seen in Figure 6. Thus, the plots in Figure 10 reflect only different behaviors of vascular tone in the microcirculatory chamber and the venous chamber.

Figure 6a reproduces the situation when all $P_{Ti}(t)$ remain unchanged during occlusion. In this case, although blood redistributes between chambers during occlusion, after cuff pressure release, the blood volume in the microcirculatory bed returns to its baseline level. PORH is not observed. Figure 6b reflects the case when $P_{Tm}(t)$ decreases exponentially (from the moment the maximum occlusion pressure $P_c(t)$ is reached) down to zero during occlusion, and after full cuff release gradually recovers. In this situation, PORH begins to manifest itself clearly. However, it is important to note that both situations do not involve changes in venous vascular tone.

The most interesting cases correspond to Figure 10c,d. To reproduce the response shown in Figure 10c, it was necessary to assume a simultaneous drop of vascular tone to zero during occlusion in both the venous chamber and the microcirculatory chamber, but with different exponential rates (in the microcirculatory chamber decreasing two times faster than in the venous chamber).

For simulating the process of the type shown in Figure 6f, with the initial enhancement of relative blood volume in the microcirculatory chamber, it was necessary to assume that the vessels' tone in the microcirculatory chamber drops sharply to zero within the first fractions of a second from the start of cuff inflation, i.e., reflexively, even before full occlusion begins. Moreover, during the occlusion, the tone must then begin to rise rapidly and exceed the initial level by about 1.5 times by the end of occlusion (a paradoxical reaction), and upon cuff release, again drop sharply to zero, gradually returning to its baseline state. An example of behavior of $P_{Tm}(t)$ modeled for this case is shown in Figure 11.

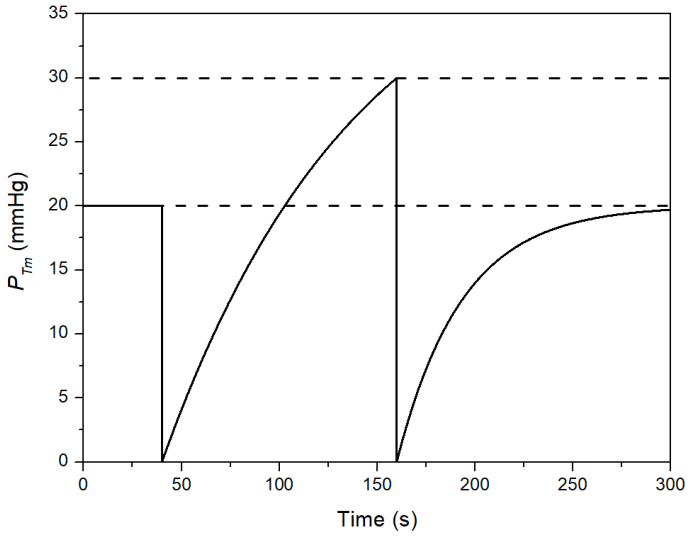

Figure 11. Example of behavior of $P_{Tm}(t)$ during occlusion to simulate the case with the initial enhancement of relative blood volume in the microcirculatory chamber.

We do not currently know whether vascular smooth muscles can physiologically respond in this way to the cuff's effect. This is a rather complex reaction at a first glance, but if one assumes dysfunction of neurogenic tone regulation—such as age-related changes or early-stage diabetic neuropathy—it appears quite plausible, in the authors' view. The model result of such a case is shown in Figure 10d. Functionally, Figures 6f and 10d seem similar. In any case, varying any other parameters during the simulation did not allow us to obtain such a signal as was actually recorded in the experiment.

4. Discussion

In our view, the physiological reactions of the microvascular bed in terms of changes in vascular tone are generally known, but the details are still poorly studied. While for

large vessels, visualization methods (angiography, ultrasound) allow assessment of the vessel lumen area and its dynamics under various conditions, until recently, physicians and physiologists had no accessible tool to study the tone and reactivity of the microvascular bed. As we showed in our literature analysis in [10], even a strict scientific definition of vascular tone did not exist until very recently. Optical methods of flowmetry and PPG open up such possibilities. However, beyond registering clinical data by optical methods (as in Figure 6), a theoretical basis is needed for their analysis and interpretation in terms of tone and reactivity. This paper does not claim to provide a final or comprehensive solution to the problem. It is only our first, pilot study. In our opinion, together with publication [10], we just have identified one possible and interesting path toward addressing the issue. To the best of our knowledge, this is the first attempt to justify the possibility of interpreting PPG signals recorded during long-term brachial artery occlusion in terms of vascular tone and reactivity. For the first time, raw PPG signals during prolonged occlusion are analyzed from this perspective.

Earlier, in [27], we had already substantiated the importance of analyzing the raw LDF signal during prolonged occlusion. Despite the fact that a different method was used earlier (LDF rather than PPG), the dynamics of the optical signal during occlusion were the same. Independently, the same dynamics of the signal during occlusion like as in Figure 10a, were reported in [26] using the PPG technique. However, at that time, the rationale was somewhat different, and we were unable to develop the idea further. In the present study, we proposed a modeling-based approach to the interpretation of these clinical data, which, in our view, is more productive.

Naturally, the proposed model is imperfect and rough. For example, it does not take into account possible changes in blood viscosity during occlusion due to erythrocyte aggregation. It also does not account for the influence of surrounding tissues on the vessels, although it is known that they affect peripheral hemodynamics during the occlusion test, as well [39]. Many other possible processes are also neither considered nor modeled.

A key distinction of our model from established models used for PB signal analysis is its representation of blood flow throughout the entire vascular bed of the arm during long-term occlusion, rather than focusing solely on the brachial artery. This fundamental difference in scope and objective precludes a direct comparison of our results with those from previous studies.

A variety of equations of state have been employed in the literature—for instance, a specific form presented in [40]:

$$S(t) = \frac{d\ln(aP(t) + b)}{1 + e^{-cP(t)}} \tag{16}$$

where a, b, c, d are constants, or the entirely different model in [41]. We acknowledge that the use of different state equations could cause different peculiarities in the calculation results—however, we maintain that the core findings of our study would not be substantially altered by such a substitution. This is due to the fact that all such equations describe a similar sigmoidal pressure-area relationship. The critical factor during occlusion is not the specific form of the equation, but the dynamic change in a key parameter within it. Moreover, the model we selected [36,37] offers a significant practical advantage: it possesses only a single parameter b, which has a clear physiological derivation from the point of maximum compliance. Alternative equations often contain multiple constants that lack an equally straightforward physiological interpretation and would require additional justification.

In addition, a significant limitation of our study is the absence of different groups of subjects with various vascular diseases and pathologies, as well as the lack of comparative results obtained by standard instrumental methods or laboratory tests of vessels and blood.

For now, unfortunately, a larger-scale study has not been feasible, since until recently there was no confidence that modeling could provide any clear and plausible results for physicians and physiologists. Now, such confidence is greater, and there are stronger grounds to plan subsequent cohort studies in this direction. Machine learning methods may also be useful in this regard. Such a study requires collecting more clinical data, which is planned for the future.

The main challenge, as we see it, should be to confirm clinically the modeling results of the type shown in Figure 10d—that vascular tone of the microcirculatory bed can indeed behave in such a way under certain conditions. At present, no alternative methods exist in clinical practice or experimental studies to measure microvascular tone in vivo. Nevertheless, in vascular physiology, rapid vascular reactions to stress, within 1–2 s, are known [38]. Registered reactions similar to Figure 6f are encountered in practice. Therefore, as a first and pilot step, our results appear interesting and open the possibility for discussion and further development of this diagnostic approach.

It seems also particularly important that, according to the theoretical results, the main contribution to the behavior of the registered optical signals comes not from the initial conditions—vessel wall stiffness, BP, etc.—but from the *dynamics* of the parameters that can change over the time interval of the occlusion test. In this study, within the stated limitations, we obtained the result that the main such parameter is vascular tone.

The most interesting and still open question, in our view, in light of the obtained results, can be formulated as follows. It is quite possible that vascular tone is dynamically adjusted to BP and vessel wall stiffness continuously, perhaps even within a single cardiac cycle, thereby keeping compliance near its maximum. In this sense, a known physiological feature of smooth muscle has not yet been incorporated into our model: when smooth muscles are rapidly stretched, their cell membranes deform and depolarization occurs, leading to the rapid stereotypical contraction of smooth muscle cells [38]. Such behavior could be taken into account in calculations, but the exact response function is still unclear, as well as its physiological relevance for each cardiac cycle. Indeed, as our modeling results showed, blood flow can be maintained even at constant tone for sufficiently long periods—on the order of tens of seconds. Thus, the functional equation for tone variation in different situations seems to be the most open question for understanding and modeling, since it is possible to select such a function to describe specific clinical results, but to grasp the physiological meaning of an individual patient's response remains a complex task.

5. Conclusions

Summing up, we can conclude the following. In this study, we developed a simplified model of hemodynamics in the upper limb to explain and interpret the behavior of the PPG signal during a prolonged arterial occlusion test. In our opinion, the model has shown quite promising initial results. Specifically, theoretical simulations have demonstrated for the first time that vascular tone in the arm's microcirculatory bed plays a key role in the dynamics of the PPG signal during occlusion.

Although this model does not describe all the aspects of blood flow in the skin of the upper limb, it makes it possible to better understand the influence of various physiological parameters of the vascular bed on the recorded PPG signal. For well-known optical diagnostic techniques such as PPG, LDF, or others, this approach is new and opens the way to a more accurate interpretation of clinical diagnostic data in terms of vascular physiology.

Furthermore, with further refinement, this model could provide clinicians and physiologists with a new, unique, and sensitive tool for studying the microvascular bed under both normal and pathological conditions.

Author Contributions: Conceptualization, D.A.R.; methodology, A.P.T. and D.A.R.; software, A.P.T. and D.A.R.; validation, A.P.T., V.N.K. and D.A.R.; formal analysis, A.P.T., V.N.K. and D.A.R.; investigation, A.P.T., V.N.K. and D.A.R.; resources, D.A.R.; data curation, A.P.T., V.N.K. and D.A.R.; writing—original draft preparation, A.P.T. and D.A.R.; writing—review and editing, A.P.T. and D.A.R.; visualization, A.P.T. and D.A.R.; supervision, D.A.R.; project administration, D.A.R.; funding acquisition, D.A.R. All authors have read and agreed to the published version of the manuscript.

Funding: This work was supported by the Russian Science Foundation, project No. 24-25-00222 (https://rscf.ru/project/24-25-00222/ (accessed on 20 November 2025)).

Institutional Review Board Statement: The study protocol complies with the ethical principles of the Declaration of Helsinki (2013 revision) and was approved by the Independent Ethics Committee of the Moscow Regional Research and Clinical Institute ("MONIKI") (Protocol No. 5, dated 21 March 2024).

Informed Consent Statement: Written informed consent was obtained from all participants.

Data Availability Statement: Data can be made available on request.

Conflicts of Interest: The authors declare no conflicts of interest.

References

1. Roth, G.A.; Mensah, G.A.; Johnson, C.O.; Addolorato, G.; Ammirati, E.; Baddour, L.M.; Barengo, N.C.; Beaton, A.Z.; Benjamin, E.J.; Benziger, C.P.; et al. Global burden of cardiovascular diseases and risk factors, 1990–2019: Update from the GBD 2019 study. *J. Am. Coll. Cardiol.* **2021**, *76*, 2982–3021. [CrossRef]
2. Luzhnov, P.V.; Pika, T.O.; Shamaev, D.M. Developing the structure of a hardware and software system for quantitative diagnosis of microhemodynamics. *Int. J. Biomed.* **2015**, *5*, 228–230. [CrossRef]
3. Rajan, V.; Varghese, B.; van Leeuwen, T.G.; Steenbergen, W. Review of methodological developments in laser Doppler flowmetry. *Lasers Med. Sci.* **2009**, *24*, 269–283. [CrossRef]
4. Kyriacou, P.A.; Allen, J. *Photoplethysmography: Technology, Signal Analysis and Applications*; Elsevier Academic Press: Amsterdam, The Netherlands, 2022.
5. Lapitan, D.; Rogatkin, D. Optical incoherent technique for noninvasive assessment of blood flow in tissues: Theoretical model and experimental study. *J. Biophotonics* **2021**, *14*, e202000459. [CrossRef]
6. Valdes, C.P.; Varma, H.M.; Kristoffersen, A.K.; Dragojevic, T.; Culver, J.P.; Durduran, T. Speckle contrast optical spectroscopy, a non-invasive, diffuse optical method for measuring microvascular blood flow in tissue. *Biomed. Opt. Express* **2014**, *5*, 2769–2784. [CrossRef]
7. Roustit, M.; Cracowski, J.L. Non-invasive assessment of skin microvascular function in humans: An insight into methods. *Microcirculation* **2012**, *19*, 47–64. [CrossRef]
8. Troy, A.M.; Cheng, H.M. Human microvascular reactivity: A review of vasomodulating stimuli and non-invasive imaging assessment. *Physiol. Meas.* **2021**, *42*, 094001. [CrossRef] [PubMed]
9. Roustit, M.; Cracowski, J.L. Assessment of endothelial and neurovascular function in human skin microcirculation. *Trends Pharmacol. Sci.* **2013**, *34*, 373–384. [CrossRef] [PubMed]
10. Rogatkin, D.A.; Ivlieva, A.L.; Shtyflyuk, M.E. Cumulative assessment of tone and reactivity of the microvascular bed based on in vivo optical flowmetry data. Justification of the approach. *Med. Fiz.* **2024**, *3*, 65–82. [CrossRef]
11. Lewis, P.S. Oscillometric measurement of blood pressure: A simplified explanation. *J. Hum. Hypertens.* **2019**, *33*, 349–351. [CrossRef] [PubMed]
12. Sharman, J.E.; Tan, I.; Stergiou, G.S.; Lombardi, C.; Saladini, F.; Butlin, M.; Padwal, R.; Asayama, K.; Avolio, A.; Brady, T.M.; et al. Automated 'oscillometric' blood pressure measuring devices: How they work and what they measure. *J. Hum. Hypertens.* **2023**, *37*, 93–100. [CrossRef]
13. Forouzanfar, M.; Dajani, H.R.; Groza, V.Z.; Bolic, M.; Rajan, S.; Batkin, I. Oscillometric blood pressure estimation: Past, present, and future. *IEEE Rev. Biomed. Eng.* **2015**, *8*, 44–63. [CrossRef]
14. Kumar, S.; Yadav, S.; Kumar, A. Accuracy of oscillometric-based blood pressure monitoring devices: Impact of pulse volume, arrhythmia, and respiratory artifact. *J. Hum. Hypertens.* **2024**, *38*, 45–51. [CrossRef]
15. Forster, F.K.; Turney, D. Oscillometric determination of diastolic, mean and systolic blood pressure—A numerical model. *J. Biomech. Eng.* **1986**, *108*, 359–364. [CrossRef]
16. Drzewiecki, G.; Hood, R.; Apple, H. Theory of the oscillometric maximum and the systolic and diastolic detection ratios. *Ann. Biomed. Eng.* **1994**, *22*, 88–96. [CrossRef] [PubMed]

17. Forouzanfar, M.; Ahmad, S.; Batkin, I.; Dajani, H.R.; Groza, V.Z.; Bolic, M. Coefficient-free blood pressure estimation based on pulse transit time–cuff pressure dependence. *IEEE Trans. Biomed. Eng.* **2013**, *60*, 1814–1824. [CrossRef] [PubMed]
18. Wang, D.; Reynolds, L.; Alberts, T.; Vahala, L.; Hao, Z. Model-based analysis of arterial pulse signals for tracking changes in arterial wall parameters: A pilot study. *Biomech. Model. Mechanobiol.* **2019**, *18*, 1629–1638. [CrossRef]
19. Raamat, R.; Talts, J.; Jagomägi, K.; Länsimies, E. Mathematical modelling of non-invasive oscillometric finger mean blood pressure measurement by maximum oscillation criterion. *Med. Biol. Eng. Comput.* **1999**, *37*, 784–788. [CrossRef]
20. Babbs, C.F. Oscillometric measurement of systolic and diastolic blood pressures validated in a physiologic mathematical model. *Biomed. Eng. Online* **2012**, *11*, 56. [CrossRef] [PubMed]
21. Barbé, K.; Van Moer, W.; Schoors, D. Analyzing the windkessel model as a potential candidate for correcting oscillometric blood-pressure measurements. *IEEE Trans. Instrum. Meas.* **2012**, *61*, 411–418. [CrossRef]
22. Kyriacou, P.A.; Shafqat, K.; Pal, S.K. Pilot investigation of photoplethysmographic signals and blood oxygen saturation values during blood pressure cuff-induced hypoperfusion. *Measurement* **2009**, *42*, 1001–1005. [CrossRef]
23. Nitzan, M.; Slotki, I.; Shavit, L. More accurate systolic blood pressure measurement is required for improved hypertension management: A perspective. *Med. Devices* **2017**, *10*, 157–163. [CrossRef]
24. Fang, H.; Xiong, J.; He, L. Fair non-contact blood pressure estimation using imaging photoplethysmography. *Biomed. Opt. Express* **2024**, *15*, 2133–2151. [CrossRef]
25. Barron, S.A.; Rogowski, Z.; Kanter, Y.; Hemli, J. DC photoplethysmography in the evaluation of sympathetic vasomotor responses. *Clin. Physiol.* **1993**, *13*, 561–572. [CrossRef]
26. Mashayekhi, G.; Zahedi, E.; Attar, H.M.; Sharifi, F. Flow mediated dilation with photoplethysmography as a substitute for ultrasonic imaging. *Physiol. Meas.* **2015**, *36*, 1551. [CrossRef]
27. Lapitan, D.G.; Rogatkin, D.A. Features of the DC component of the laser Doppler signal during arterial occlusion. In Proceedings of the 2018 International Conference Laser Optics (ICLO), Saint Petersburg, Russia, 4–8 June 2018; p. 514. [CrossRef]
28. Lapitan, D.G.; Raznitsyn, O.A. A method and a device prototype for noninvasive measurements of blood perfusion in a tissue. *Instrum. Exp. Tech.* **2018**, *61*, 745–750. [CrossRef]
29. Glazkov, A.A.; Lapitan, D.G.; Makarov, V.V.; Rogatkin, D.A. Optical non-invasive automated device for the study of central and peripheral hemodynamics. *Phys. Bases Instrum.* **2021**, *10*, 28–36. [CrossRef]
30. Lapitan, D.G.; Tarasov, A.P.; Rogatkin, D.A. Justification of the photoplethysmography sensor configuration by Monte Carlo modeling of the pulse waveform. *J. Biomed. Photonics Eng.* **2022**, *8*, 030306. [CrossRef]
31. Tarasov, A.P.; Rogatkin, D.A. Modeling of pulse wave signals for a blood pressure monitor with a remote photoplethysmography sensor. In Proceedings of the 2025 Photonics & Electromagnetics Research Symposium (PIERS), Chiba, Japan, 5–9 November 2025.
32. Saeed, F.; Carter, C.; Kolade, J.; Brothers, R.M.; Liu, H. Understanding metabolic responses to forearm arterial occlusion measured with two-channel broadband near-infrared spectroscopy. *J. Biomed. Opt.* **2024**, *29*, 117001. [CrossRef] [PubMed]
33. Smith, B.; Chase, J.; Nokes, R.; Shaw, G.; Wake, G. Minimal haemodynamic system model including ventricular interaction and valve dynamics. *Med. Eng. Phys.* **2004**, *26*, 131–139. [CrossRef] [PubMed]
34. Caro, C.G.; Pedley, T.J.; Schroter, R.C.; Seed, W.A.; Parker, K.H. *The Mechanics of the Circulation*; Oxford University Press: New York, NY, USA, 1978.
35. Volobuev, A.N. Fluid flow in tubes with elastic walls. *Phys.-Uspekhi* **1995**, *38*, 169–178. [CrossRef]
36. Hughes, D.J.; Babbs, C.F.; Geddes, L.A.; Bourland, J.D. Measurements of young's modulus of elasticity of the canine aorta with ultrasound. *Ultrason. Imaging* **1979**, *1*, 356–367. [CrossRef]
37. Hardy, H.H.; Collins, R.E. On the pressure-volume relationship in circulatory elements. *Med. Biol. Eng. Comput.* **1982**, *20*, 565–570. [CrossRef] [PubMed]
38. Hall, J.E.; Guyton, A.C. *Textbook of Medical Physiology*, 13th ed.; Elsevier Science: Philadelphia, PA, USA, 2011.
39. Lan, H.; Al-Jumaily, A.M.; Lowe, A.; Hing, W. Effect of tissue mechanical properties on cuff-based blood pressure measurements. *Med. Eng. Phys.* **2011**, *33*, 1287–1292. [CrossRef] [PubMed]
40. Forouzanfar, M.; Dajani, H.R.; Groza, V.Z.; Bolic, M.; Rajan, S.; Batkin, I. Ratio-independent blood pressure estimation by modeling the oscillometric waveform envelope. *IEEE Trans. Instrum. Meas.* **2014**, *63*, 2501–2503. [CrossRef]
41. Chandrasekhar, A.; Yavarimanesh, M.; Hahn, J.O.; Sung, S.H.; Chen, C.H.; Cheng, H.M.; Mukkamala, R. Formulas to explain popular oscillometric blood pressure estimation algorithms. *Front. Physiol.* **2019**, *10*, 1415. [CrossRef]